RESEARCH ARTICLE OPEN ACCESS

ATP1A3 Disease Spectrum Includes Paroxysmal Weakness and Encephalopathy Not Triggered by Fever

Chetan Immanneni, BA,* Daniel Calame, MD, PhD,* Song Jiao, PhD, Lisa T. Emrick, MD, Miguel Holmgren, PhD, and Sho T. Yano, MD, PhD

Correspondence
Dr. Holmgren
holmgren@ninds.nih.gov
or Dr. Yano
syano@uchicago.edu

Neurol Genet 2024;10:e200150. doi:10.1212/NXG.0000000000200150

Abstract

Background and Objectives

Heterozygous pathogenic variants in *ATP1A3*, which encodes the catalytic alpha subunit of neuronal Na^+/K^+-ATPase, cause primarily neurologic disorders with widely variable features that can include episodic movement deficits. One distinctive presentation of *ATP1A3*-related disease is recurrent fever-triggered encephalopathy. This can occur with generalized weakness and/or ataxia and is described in the literature as relapsing encephalopathy with cerebellar ataxia. This syndrome displays genotype-phenotype correlation with variants at p.R756 causing temperature sensitivity of ATP1A3. We report clinical and in vitro functional evidence for a similar phenotype not triggered by fever but associated with protein loss-of-function.

Methods

We describe the phenotype of an individual with de novo occurrence of a novel heterozygous *ATP1A3* variant, NM_152296.5:c.388_390delGTG; p.(V130del). We confirmed the pathogenicity of p.V130del by cell survival complementation assay in HEK293 cells and then characterized its functional impact on enzymatic ion transport and extracellular sodium binding by two-electrode voltage clamp electrophysiology in *Xenopus* oocytes. To determine whether variant enzymes reach the cell surface, we surface-biotinylated oocytes expressing N-tagged ATP1A3.

Results

The proband is a 7-year-old boy who has had 2 lifetime episodes of paroxysmal weakness, encephalopathy, and ataxia not triggered by fever. He had speech regression and intermittent hand tremors after the second episode but otherwise spontaneously recovered after episodes and is at present developmentally appropriate. The p.V130del variant was identified on clinical trio exome sequencing, which did not reveal any other variants possibly associated with the phenotype. p.V130del eliminated ATP1A3 function in cell survival complementation assay. In *Xenopus* oocytes, p.V130del variant Na^+/K^+-ATPases showed complete loss of ion transport activity and marked abnormalities of extracellular Na^+ binding at room temperature. Despite this clear loss-of-function effect, surface biotinylation under the same conditions revealed that p.V130del variant enzymes were still present at the oocyte's cell membrane.

Discussion

This individual's phenotype expands the clinical spectrum of *ATP1A3*-related recurrent encephalopathy to include presentations without fever-triggered events. The total loss of ion transport function with p.V130del, despite enzyme presence at the cell membrane, indicates that haploinsufficiency can cause relatively mild phenotypes in *ATP1A3*-related disease.

*These authors are co-first authors.

From the Sam Houston State University College of Osteopathic Medicine (C.I.), Conroe, TX; Molecular Neurophysiology Unit (C.I., S.J., M.H.), National Institute of Neurological Diseases and Stroke, National Institutes of Health, Bethesda, MD; Section of Pediatric Neurology and Developmental Neuroscience (D.C.), Department of Pediatrics; Department of Molecular and Human Genetics (D.C., L.T.E.), Baylor College of Medicine; Texas Children's Hospital (D.C.), Houston, TX; National Human Genome Research Institute (S.T.Y.), National Institutes of Health, Bethesda, MD; and Section of Pediatric Neurology (S.T.Y.), Department of Pediatrics, University of Chicago, IL.

Go to Neurology.org/NG for full disclosures. Funding information is provided at the end of the article.

The Article Processing charge was funded by the authors.

Glossary

AHC = alternating hemiplegia of childhood; **ES** = exome sequencing; **FIPWE** = fever-induced paroxysmal weakness and encephalopathy; **RECA** = relapsing encephalopathy with cerebellar ataxia.

Introduction

ATP1A3 encodes the neuronally expressed α3 subunit of the sodium-potassium ATPase (Na^+/K^+-ATPase), a P-type ATPase responsible for generating electrochemical gradients of Na^+ and K^+ across the cell membrane. These gradients power essential functions such as action potentials, clearance of intracellular calcium, and cotransport of other substrates.[1] Accordingly, α3 is highly expressed in the brain in various mixtures with other α isoforms.[2] Heterodimerization of one α with one β subunit is sufficient to assemble the core Na^+/K^+-ATPase, which is regulated by additional γ subunits. This complex exports 3 intracellular Na^+ in exchange for the import of 2 extracellular K^+ and consumes 1 ATP per reaction cycle.[1]

Heterozygous pathogenic variants in *ATP1A3* are associated with a wide spectrum of neurologic diseases. Frequently observed phenotypes include alternating hemiplegia of childhood (AHC), rapid-onset dystonia-parkinsonism, and CAPOS (cerebellar ataxia, areflexia, pes cavus, optic atrophy, sensorineural hearing loss) syndrome.[3–6] However, other phenotypes of highly variable severity are emerging, ranging from congenital malformation and brain atrophy to isolated auditory neuropathy.[7–10] Although the level of enzyme activity alone does not account for disease severity, some *ATP1A3* genotypes clearly correlate with phenotype.[11,12] Thus, characterization of the full spectrum of *ATP1A3* phenotypes along with the molecular consequences of the associated variants is important to recognize patterns of disease in the clinic, prognosticate based on genotype, understand disease pathogenesis, and develop precision therapeutics.

One such *ATP1A3*-related syndrome correlated with genotype is defined by recurrent fever-triggered episodes of acute encephalopathy followed by slow recovery. Because episodes can involve symmetric weakness and/or ataxia, this has been referred to as relapsing encephalopathy with cerebellar ataxia (RECA) or fever-induced paroxysmal weakness and encephalopathy (FIPWE).[13,14] This phenotype can overlap with other *ATP1A3*-related conditions such as AHC and CAPOS in which febrile illness or temperature changes can also trigger encephalopathy. However, patients with those conditions typically have other, more prominent features, such as more frequent episodes of asymmetric movement disorders and greater nonparoxysmal neurologic impairment in AHC, or the titular features of CAPOS syndrome. RECA is consistently found in patients with variants at ATP1A3 residue p.R756 including p.R756H, which induces temperature-sensitive misfolding of α3 protein.[13]

We describe the clinical phenotype and experimental investigation of *ATP1A3* p.V130del. This variant occurred in a patient with 2 episodes of encephalopathy like those in RECA but not triggered by fever. Functional studies in vitro showed that p.V130del both eliminates electrogenic ion transport by α3 Na^+/K^+-ATPase and disrupts extracellular Na^+ binding/unbinding, but does not prevent α3 from being produced and reaching the cell membrane. These findings expand the phenotypic spectrum of *ATP1A3*-related recurrent encephalopathy and molecular spectrum of disease variants.

Methods

Data Availability

Raw data for in vitro experiments are available from the corresponding author upon reasonable request. Clinical details beyond those already included in the article will not be provided because of identifiability and privacy concerns.

Standard Protocol Approvals, Registrations, and Patient Consents

The patient's guardian provided written informed consent for study participation and publication under Baylor College of Medicine Institutional Review Board protocol H-29697. The family underwent clinical trio exome sequencing (ES) at GeneDx.

Constructs

We used the NM_152296.5 (*ATP1A3*) and NM_001677.4 (*ATP1B1*) reference transcripts. All *ATP1A3* constructs contained 2 ouabain-resistance variants, c.323A>G;p.(Q108R)/c.355A>G;p.(N119D), to distinguish expressed *ATP1A3* from endogenous Na^+/K^+-ATPases.[15] They were subcloned into pGEMHE for cRNA synthesis[16] and pcDNA3.1+ (Thermo Fisher) for transfection. p.D801N and p.V130del variants were introduced in pGEMHE by cloning overlap-extension PCR products using the following primer pairs into the MfeI/HindIII (D801N) or BamHI/DraIII (V130del) sites on the same construct: D801N: CATTCCCGTCAGCCAGGTTA (forward/c.1917), CAGTGCCCAGATTGATGCAGAG (reverse, D801N); CTCTGCATCAATCTGGGCACTG (forward/D801N), TATGTAGCTTAGAGACTCCATTCGG (reverse/vector); V130del: GCTCAGAATAAACGCTCAACTTTGG (forward/vector), GTAGGAGAAGCAGCCAGTGATGAtcACGGCCGCCAGCACGATGCCCAGG (reverse/V130del); CCTGGGCATCGTGCTGGCGGCCGTgaTCATCACTGGCTGCTTCTCCTAC (forward, V130del), GAGGCTGGTTTAGTGGTAACC (reverse/vector).

For Western blotting in oocytes, an N-terminal tag consisting of the following sequence elements was introduced in frame

between the first and second codons: EcoRI site, 3xFLAG-Strep (nt 2611-2784 of Addgene 68375), 7-residue spacer (GGCTCGAGCGGAGGCTCTAGA), mCherry (nt 1747-2451 of Addgene 41583), 11-residue spacer (GGTGGTT-CTGGTGGTGGTTCTGGTGGGTCGAGC). Plasmid 68375, AAVS1_Puro_PGK1_3xFLAG_Twin_Strep, was a gift from Yannick Doyon (Addgene plasmid 68375[17]; RRID:Addgene_68375),[18] and 41583, pCAGGS-mCherry, was a gift from Phil Sharp (Addgene plasmid 41583[19]; RRID:Addgene_41583).[20]

Ouabain Survival Assay for Cell Survival Analysis

We grew 1.5 × 10^5 HEK293 cells/well in 12-well plates overnight in 2 mL DMEM/F12 medium (37°C, 5% CO_2). We transfected 900 μg/well ouabain-resistant *ATP1A3* expression constructs using 1.35 μL lipofectamine 3000 with 1.8 μL P3000 (Thermo Fisher). After 2 days, we detached cells in 500 μL TrypLE (Gibco), added 4 mL medium, centrifuged at 130*g* for 5 minutes, resuspended the cells in medium, split the culture into two 2 mL wells, and added 10 μM ouabain to one well. After 2 days, we washed once with 1 mL phosphate-buffered saline pH 7.4 (Gibco) to remove dead nonadherent cells, detached surviving cells in 1 mL TrypLE, and counted them in a CellDrop (DeNovix).

We calculated cell survival by dividing the number of cells that survived with ouabain by the number of cells that survived without ouabain. We compared wildtype with each other condition using Dunnett test for multiple comparisons.

Oocyte Injection and Incubation

We synthesized coding RNAs (cRNAs) using the mMESSAGE mMACHINE T7 Ultra Kit (Thermo Fisher). We injected defolliculated *Xenopus laevis* oocytes (Ecocyte) with 36.8 nL cRNA mixture containing 36.8 ng *ATP1A3* and 12.3 ng *ATP1B1* cRNA and incubated for 2–3 days at 16°C in ND96 solution (96 mM NaCl, 2 mM KCl, 1 mM $MgCl_2$, 1.8 mM $CaCl_2$, 5 mM HEPES, 100 mg/L gentamicin, pH 7.6).

Two-Electrode Voltage Clamp Electrophysiology

We used a two-electrode voltage clamp to investigate electrogenic ion transport and extracellular Na^+ ion binding. We incubated the oocytes in Na^+-loading solution (110 mM NaCl, 2.5 mM Na-citrate, 5 mM HEPES, 2 μM ouabain, pH 7.6) for 1–3 hours at room temperature before recording. Recordings were performed at room temperature using electrodes filled with 3 M KCl.

All extracellular solutions[15] contained 2 μM ouabain, 110 mM NaOH, 0.3 mM niflumic acid, 5 mM HEPES, 5 mM 1 M $BaCl_2$, 2 mM 1 M $NiCl_2$, 2 mM 1 M $MgCl_2$, and methanesulfonic acid to pH 7.6 with either 5 mM additional NaCl (0 mM K^+ solution) or 5 mM KCl (5 mM K^+ solution).

The holding voltage was 0 mV. Time controls and solution changes were done at 2-minute intervals. We perfused 0 mM K^+ solution until holding current was stable and time controls showed ≤20 nA difference at any voltage. We then perfused 5 mM K^+ solution with 2 μM ouabain followed by the same solution with 10 mM ouabain and calculated Na^+/K^+-ATPase steady-state currents by subtracting the 2 measurements at 5 mM K^+ (2 μM - 10 mM ouabain). We then took a time control in 10 mM ouabain solution and washed out ouabain by perfusing 0 mM K^+ solution for 9 minutes. We then measured Na^+-K^+-ATPase sodium transient currents by performing the same measurements and subtraction at 0 mM K^+ (2 μM - 10 mM ouabain).

Steady-state currents were measured using 100 ms pulses ranging from −100 to +30 mV in 10 mV increments. Transient currents were measured using 50 ms pulses ranging from −160 to +40 mV in 10 mV increments, followed by 150 ms relaxation at 0 mV. Data were acquired at a sampling frequency of 20 kHz through a Frequency Devices 900 lowpass filter set to 5 kHz using an Axon Digidata 1550 acquisition system, with continuous monitoring using Axon MiniDigi 1B.

Analysis was performed using pCLAMP software (Molecular Devices) and GraphPad Prism 9. Steady-state currents were calculated by taking the average of the current between 50 and 100 ms of the recording (approximately the last half of the voltage pulse). To calculate transient currents, recordings were filtered through a 1-kHz lowpass filter and background current was subtracted (average of last 5 ms of trace). We calculated the charge moved by the off-transient currents, representing movement of ions induced by return of the voltage to zero, by integrating the monoexponential decay curve fit of each transient currents. For each oocyte, we calculated the mean time constant at the 3 most negative voltages (−160 to −140 mV) and fit all currents to a monoexponential decay function using that time constant. Because of the slow clamp time of the two-electrode system, we fit transient currents starting 4 ms after the end of the pulse and extrapolated the fit to the beginning of the pulse.

Western Blot

Oocytes that had not been impaled for electrophysiology were used, either expressing N-tagged *ATP1A3* and *ATP1B1* cRNAs (injected as above) or uninjected as negative controls.

To extract total protein, batches of 5 oocytes were washed twice with ND96, resuspended in 100 μL precooled buffer H (1% Triton X-100, 100 mM NaCl, 20 mM Tris-HCl, and protease inhibitor cocktail, pH 7.4) at 4°C, and lysed/homogenized by pipetting up and down 10–20 times.[21] Lysates were centrifuged at 10,000×*g* for 5 minutes at 4°C to separate yolk, supernatant, and pellet. The supernatants were collected and analyzed by Western blot.

To separate surface and intracellular proteins, batches of 10 oocytes were surface-biotinylated in 12-well plates as described.[22] Briefly, all steps were performed at 4°C. Oocytes were washed with ND96 buffer 3 times and incubated for 1

hour in biotinylation buffer (10 mM triethanolamine, 150 mM NaCl, 2 mM $CaCl_2$, 1 mg/mL EZ-Link Sulfo-NHS-Biotin (Thermo Fisher A39256), pH 9.5) with gentle agitation. To stop biotinylation, oocytes were washed twice with quench buffer (ND96 supplemented with 192 mM glycine and 25 mM Tris-HCl, pH 7.5). After the second wash, oocytes were incubated in the quench buffer for 5 minutes with gentle agitation, followed by 2 washes with ND96. Oocytes were then lysed in 200 μL of buffer H, homogenized by pipetting, rotated at 4°C for 5 minutes, and centrifuged at 10,000×*g* for 5 minutes. To pull down biotinylated proteins, 150 μL of the supernatant was diluted with 75 μL of buffer H, added to 50 μL of Pierce Avidin Agarose (Thermo Fisher 20219), which had been previously washed twice with buffer H, and incubated for 1 hour with gentle agitation. After incubation, the samples were centrifuged at 3,000×*g* for 3 minutes. The supernatant was collected as the unbound fraction, which contained nonbiotinylated proteins. After the resin was washed 6 times with lysis buffer, 40 μL of 2x SDS sample buffer (Thermo Fisher LC2676) was added, vortexed, and heated at 95°C for 5 minutes followed by centrifugation. The supernatant was collected as the bound fraction, which contained biotinylated proteins. 20 μL aliquots from 225 μL unbound fraction and 10 μL aliquots from 40 μL bound fraction were analyzed by Western blot.

Immunoblotting was performed using the standard protocol. Blots transferred from sodium dodecyl sulfate-polyacrylamide gel electrophoresis were cut in half for detection of ATP1A3 bands in the top half and α-tubulin bands in the bottom half. Mouse anti-Strep antibody (CAT 34850, Qiagen) and mouse anti-α-tubulin (CAT ab7291, Abcam) were used to detect Strep-tagged ATP1A3 proteins and α-tubulin, respectively. Donkey anti-mouse HRP-conjugated secondary antibodies (CAT 711-035-151, Jackson ImmunoResearch) and ECL reagents (CAT 32109, Thermo Fisher) were used for protein detection by chemiluminescence. Protein bands were quantified by densitometric analysis using ImageJ software (v1.52h, NIH) to measure the band intensities of ATP1A3 and α-tubulin within each individual sample. For the biotinylation assay, percentages of surface ATP1A3 among total expressed protein were estimated by dividing the ATP1A3 signals from the bound fractions by the ATP1A3 signals from both the unbound fractions and the bound fractions, described by the equation:

$$\text{Percent} = \frac{\frac{40\ \mu L}{10\ \mu L} * \text{Intensity}_{\text{bound}}}{\frac{40\ \mu L}{10\ \mu L} * \text{Intensity}_{\text{bound}} + \frac{225\ \mu L}{20\ \mu L} * \text{Intensity}_{\text{unbound}}}$$

where $\text{Intensity}_{\text{bound}}$ and $\text{Intensity}_{\text{unbound}}$ are the intensity of ATP1A3 bands from the bound fractions and the unbound fractions, respectively. For the rest of the immunoblotting assays, ATP1A3 signals were normalized to internal standard α-tubulin from the same lane, and then, the results were normalized against the wildtype groups. This experiment was repeated 3 times. All data are represented as means, and error bars indicate standard deviations. Statistical significance was determined by Student *t* test. A *p* value <0.05 was considered statistically significant. The number of independent experimental repetitions is represented by n.

Results

An Individual With Recurrent Neurologic Dysfunction has a p.V130del Variant

The patient is a 7-year-old boy with 2 lifetime episodes of encephalopathy, weakness, and ataxia. The first episode occurred when 11 months old over an approximately 24-hour period. The episode began with 2 brief spells consisting of behavioral arrest and staring without gaze deviation lasting less than one minute each. The 2 spells were separated by several hours, and in between, he returned to his baseline. The third spell was prolonged and resulted in overnight hospitalization. He was awake but did not respond to stimuli. He had purposeless roving eye movements and dilated pupils. His gaze was dysconjugate. There was no apnea, oxygen desaturations, or nystagmus. Hemiplegia or quadriplegia was not appreciated. He eventually fell asleep and immediately returned to his baseline the next morning upon waking up.

The second episode of encephalopathy, generalized weakness, and ataxia occurred when 4 years old and lasted 2 weeks. The degree of encephalopathy and weakness fluctuated throughout the illness but was not improved by sleep. There was no evidence of hemiplegia. At hospital discharge, he remained weak and had slurred speech. It took much of the following year to return to normal. There was no history of developmental delay. Neither episode was preceded by fever or associated with febrile illness, infection, headaches, or other triggers.

He is at present in the first grade. He struggles with fine motor skills because of intermittent tremulousness. The tremulousness is brief and lacks triggers. It has not been witnessed or captured on video, and therefore, it is unclear whether it represents episodic ataxia or paroxysmal tremor. He is otherwise doing well in regular classes. Outside of the paroxysmal encephalopathy, for several years, he had recurrent unexplained fevers every 3 weeks. The fevers began after the second encephalopathic episode. He exhibits minimal symptoms and only occasionally complains of arm and leg pain. Temperatures are as high as 103–105° F. Fevers last from hours up to an entire day. Abortive steroids for presumptive periodic fever syndrome were prescribed; a positive response was reported. Rheumatologic workup was negative.

Workup including brain CT and MRI, CSF studies including glucose, cell counts, bacterial culture, Mayo autoimmune encephalitis antibody panel, and neurotransmitters, and multiple prolonged electroencephalograms were all normal. Clinical trio whole-exome sequencing at GeneDx identified the de novo *ATP1A3* variant NM_152296.5:c.388_

390delGTG; p.(V130del). The variant is absent from gnomAD and ClinVar. No other pathogenic or candidate variants were reported in genes related to the patient's phenotype, including any genes associated with autoinflammation/innate immune abnormalities. We considered episodic encephalopathy with symmetric weakness and ataxia consistent with an *ATP1A3*-related disease phenotype while the episodic fevers were possibly but not clearly consistent. Autonomic dysfunction is known to occur in *ATP1A3*-related disease, but we are not aware of other reports of periodic unexplained fevers in these patients.

Val129-Val130 are highly conserved among vertebrates and are located within transmembrane helix M2 of the ion-binding domain (Figure 1, A and B, visualized on RCSB PDB structure 3WGU[24] in ChimeraX[25] and Multiz alignment from the UCSC Genome Browser).[26–28]

Based on this clinical information, p.V130del met 2 moderate and 1 supporting criteria for pathogenicity.[29] This in-frame deletion changed protein length (PM4), it was de novo with confirmed parentage in the proband, who had a somewhat specific phenotype (PS2_Moderate), and it was absent in population databases (PM2_Supporting).

p.V130del Is Likely Pathogenic

To test whether the p.V130del variant has a deleterious functional effect, we performed an ouabain cell survival assay. Ouabain specifically blocks Na^+/K^+-ATPase activity essential for cell survival and consequently kills cells.[5] Expression of partially ouabain-resistant ATP1A3 rescues cell survival while expression of ATP1A3 with disease variants does not. Therefore, we transfected HEK293 cells with partially ouabain-resistant ATP1A3 expression constructs (wildtype, p.D801N, p.V130del) and measured their ability to restore cell survival in ouabain. We confirmed ouabain killing with a mock-transfected negative control, in contrast to rescue by wildtype ATP1A3 (45.5% of the cell count without ouabain) (Figure 2A). Compared with wildtype, p.V130del-transfected cells showed significantly less survival ($p = 0.0008$ corrected for multiple comparisons), similar to the known pathogenic AHC variant p.D801N (Figure 2A). Therefore, the p.V130del variant has a deleterious functional effect, which causes Na^+/K^+-ATPases to be unable to support cell survival.

We interpreted this result as supporting evidence for pathogenicity (PS3_Supporting) under the ClinGen Sequence Variant Interpretation working group recommendations.[30] Therefore, a total of 2 moderate and 2 supporting criteria for pathogenicity apply to p.V130del, leading to interpretation of the variant as likely pathogenic.

p.V130del Eliminates Na^+/K^+-ATPase Electrogenic Ion Transport

The enzymatic function of the Na^+/K^+-ATPase is electrogenic ion transport, which generates an outward "pump current" of one positive charge per reaction cycle. To test this ability in human ATP1A3-containing Na^+/K^+-ATPase, we expressed the enzyme in *Xenopus* oocytes and used a two-electrode voltage clamp to measure pump current stimulated

Figure 1 Identification of the ATP1A3 p.V130del Variant in an Individual With Recurrent Neurologic Deficits

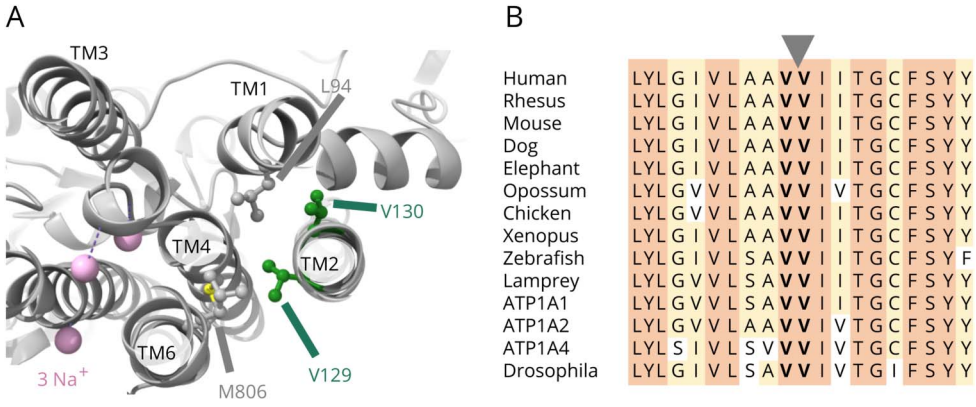

(A) Location of p.V130 within transmembrane helix M2 of the ion-binding domain. The paralogous valine within the crystal structure of the highly homologous ATP1A1 isoform (RCSB PDB 3WGU) is shown in 3D visualization using ChimeraX. The labels indicate adjacent transmembrane helices (TM), nearby side chains numbered according to the human ATP1A3 sequence, and the locations of the 3 bound Na^+. The side chain of p.V129 neighbors that of p.M806 in TM6, a residue implicated in AHC. The side chain of p.V130 neighbors that of p.L94 in TM1; the paralog of p.L94 in *ATP1A1*, p.L104, has also been implicated in disease, and the disease variant at this position (p.L104R) introduces an inward ion leak.[23] (B) Conservation of the 2 valines at p.V129-V130. Orthologous ATP1A3 protein sequences from the indicated vertebrates are shown in alignment with the valines in bold beneath the arrow. Owing to a gene duplication event in teleost fish, the zebrafish sequence shown is from Atp1a3a. At the bottom, the invertebrate *Drosophila* ortholog Atpalpha is shown for comparison along with the 3 human paralogs, ATP1A1, ATP1A2, and ATP1A4.

Figure 2 p.V130del Causes Loss of Electrogenic Ion Transport by ATP1A3

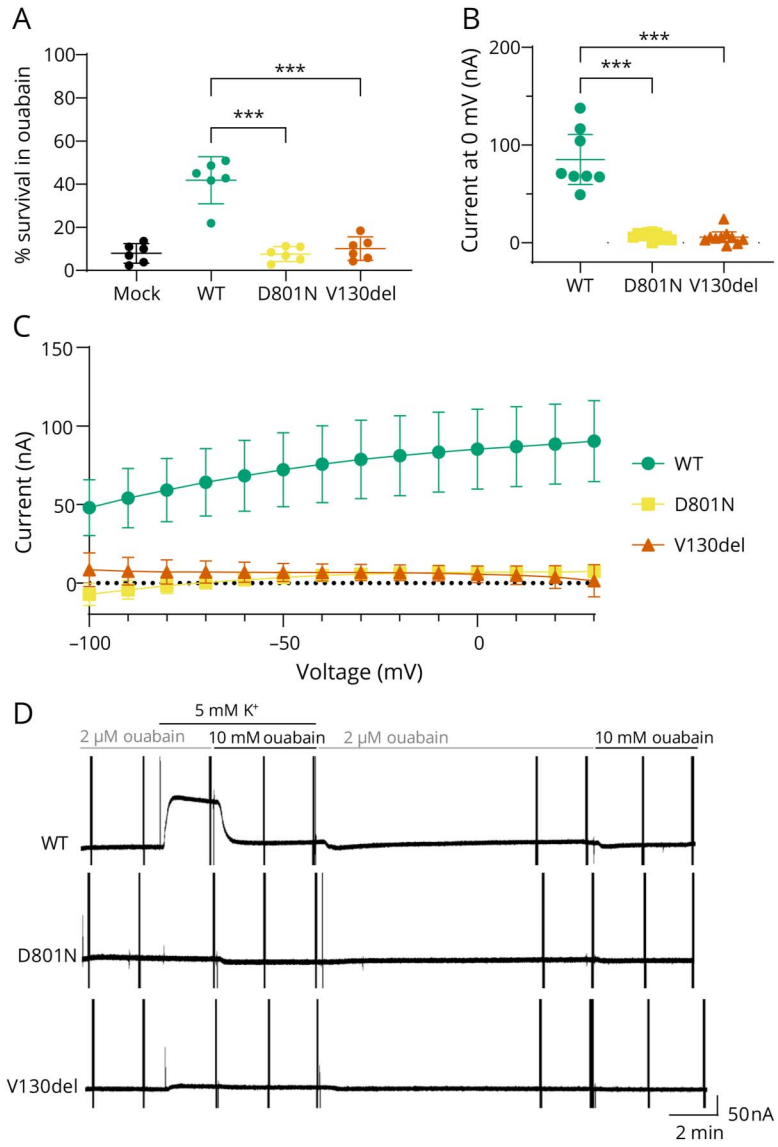

(A) Ouabain complementation assay shows a loss-of-function effect of p.V130del. HEK293 cells were transfected with expression constructs carrying partially ouabain-resistant wildtype or variant ATP1A3 as indicated for 2 days before challenge with ouabain. Cell survival in the presence of ouabain is shown normalized to the cell count in the absence of ouabain from the same transfection. p.V130del rescued significantly less cell survival than wildtype. Error bars shown in all figures are means ± 95% confidence intervals. ***$p < 0.001$. (B) p.V130del causes loss of electrogenic ion transport activity at 0 mV. Steady-state ouabain-sensitive currents generated by ATP1A3-Na^+/K^+-ATPase in the presence of 5 mM extracellular K^+ were measured using a two-electrode voltage clamp in *Xenopus* oocytes. $p = 0.0002$ for the difference between V130del and wildtype. ***$p < 0.001$. (C) p.V130del ATP1A3-Na^+/K^+-ATPase is inactive across the range of tested voltages. Steady-state ouabain-sensitive currents, as in (B), are plotted against voltage. The average of 10 replicates is shown for each construct. (D) Holding currents at 0 mV show that p.V130del ATP1A3-Na^+/K^+-ATPases are inactive, not ouabain-resistant. The entirety of the representative two-electrode voltage clamp recording is shown for each wildtype or variant ATP1A3 indicated. If the absence of ouabain-sensitive currents with p.V130del ATP1A3-Na^+/K^+-ATPases in (C) was due to decreased affinity for ouabain, then the enzyme would still generate electrogenic ion transport currents that depend on the presence of extracellular K^+. However, holding currents with p.V130del are essentially identical in the presence or absence of K^+ (compare before and after the black bar, 5 mM K^+), indicating that p.V130del ATP1A3-Na^+/K^+-ATPases do not generate ion transport currents.

by 5 mM extracellular K^+. To isolate pump currents generated by the human Na^+/K^+-ATPase, we expressed partially ouabain-resistant constructs and then measured currents in the presence of both low (2 μM) and high (10 mM) concentrations of ouabain. Endogenous *Xenopus* Na^+/K^+-ATPase activity was blocked by low ouabain (2 μM) while high ouabain (10 mM) also blocked the activity of the expressed Na^+/K^+-ATPases. Subtracting steady-state current in high ouabain from current with low ouabain yielded steady-state pump current from the ATP1A3 Na^+/K^+-ATPases.

Wildtype ATP1A3 generated positive pump currents, which were nonexistent with p.V130del (Figure 2, B and C) as well as the positive control, p.D801N, which was known to cause loss-of-function.[31] One possible explanation for loss of ouabain-sensitive pump current with p.V130del could be that the enzyme became more ouabain-resistant and remained active at both low and high ouabain concentrations. Since Na^+/K^+-ATPase requires extracellular K^+ for activity and is inactive in its absence, any such ouabain-resistant pump current would be detectable as an increase in response to extracellular K^+. However, examination of steady-state currents in low ouabain showed no change in response to extracellular K^+, demonstrating that this was not the case (Figure 2D). Therefore, p.V130del Na^+/K^+-ATPase enzymes have complete loss of electrogenic ion transport ability.

ATP1A3 p.V130del Shows Abnormal Na^+/K^+-ATPase Sodium Binding

Next, we asked whether p.V130del affects the ability of the Na^+/K^+-ATPase to bind extracellular Na^+. Unbinding/rebinding of Na^+ as it is released toward the extracellular side is normally the most voltage-dependent step of the Na^+/K^+-ATPase ion transport cycle. It can be detected in the form

of transient currents induced by voltage changes. To study transient currents by using a two-electrode voltage clamp, ouabain was washed out after measurement of pump currents in the oocytes discussed above and low/high ouabain subtractions were repeated in the absence of extracellular K^+.

Under these conditions, changes in voltage shifted the equilibrium of Na^+ binding, with more negative voltages driving Na^+ into its binding sites. We quantified the off-transient currents following each voltage pulse, representing Na^+ movement in response to the shift back from the applied voltage to 0 mV (Figure 3A). Owing to the relatively slow speed of the two-electrode voltage clamp, these currents primarily reflected the transition between 3 bound Na^+ and 2 bound Na^+, which is the slowest of the 3 binding/unbinding steps (the "slow component").[15] We fit transient currents to a monoexponential decay curve and integrated them over time to estimate the amount of charge moved.

While wildtype, p.D801N, and p.V130del Na^+/K^+-ATPases all generated detectable extracellular Na^+ transient currents, these currents were at a much lower amplitude with p.V130del and decayed with faster time constants (Figure 3, A and B). Wildtype and p.D801N enzymes displayed sigmoidal relationships between charge moved and voltage, as expected, because Na^+ binding to Na^+/K^+-ATPase follows a Boltzmann distribution. By contrast, the charge-voltage relationship with p.V130del appeared to be shifted too far to the right to determine the positive asymptote (Figure 3B, right), although our analysis was limited by the small current amplitude. These results indicated that either very small amounts of p.V130del Na^+/K^+-ATPases reach the cell surface, or p.V130del disrupts Na^+ binding and severely reduces the slow component of the Na^+ transient current.

ATP1A3 p.V130del Is Expressed and Reaches the Cell Surface

To directly confirm that the p.V130del variant protein is expressed, we performed Western blot on oocytes expressing N-terminally FLAG-Strep-mCherry-tagged ATP1A3. The tag did not interfere with enzyme function because ion transport currents measured using all 3 tagged constructs were the same as with untagged constructs (Figure 4A; compare Figure 2C). Wildtype, p.D801N, and p.V130del were all clearly expressed (Figure 4B), indicating that the observed loss-of-function was not due to total loss of protein.

To determine whether p.V130del ATP1A3 reached the cell surface under the conditions we used for the electrophysiologic measurements described above, we biotinylated surface proteins using a membrane-impermeable reagent and separated the surface from intracellular proteins by avidin pull-down. Wildtype, p.D801N, and p.V130del ATP1A3 were all present at the cell surface, with clear bands on Western blot of the biotinylated surface fraction (Figure 4C, top right). There was no off-target binding of Strep-tagged ATP1A3 to the eukaryotic avidin column in a nonbiotinylated negative control (not shown). To confirm that intracellular proteins were not biotinylated or carried over into the avidin-bound fraction, we cut each blot in half and probed the bottom half using a primary antibody against α-tubulin, which has many solvent-accessible lysines, as a cytoplasmic control. Tubulin was

Figure 3 Extracellular Na^+ Transient Currents Are Abnormal With p.V130del

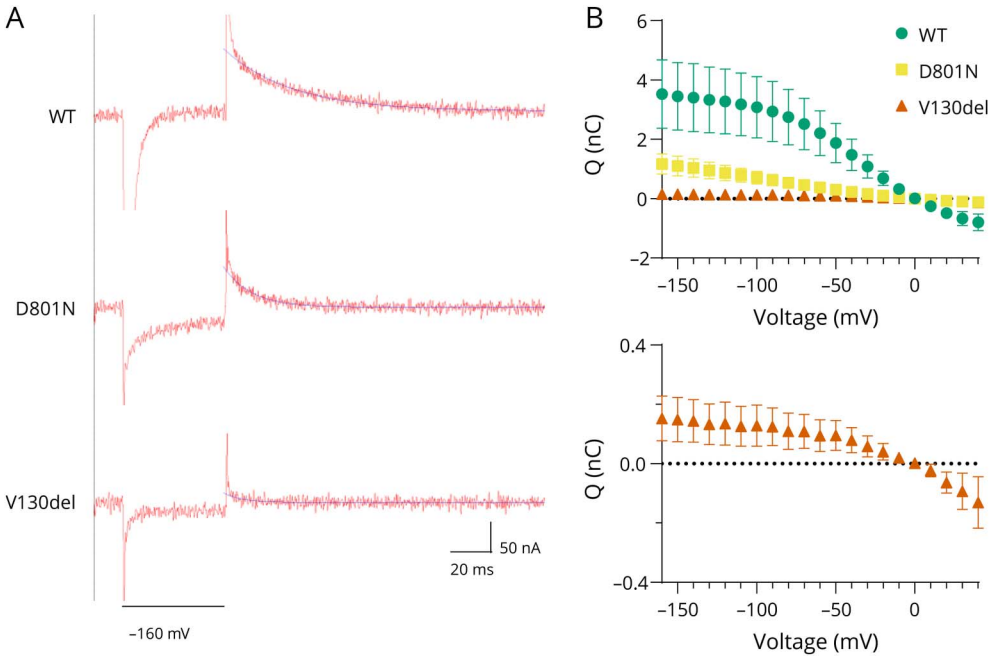

(A) Representative tracings of extracellular Na^+ transient currents induced by voltage pulses from the holding potential of 0 mV to −160 mV in the absence of extracellular K^+. Low-high ouabain subtractions from oocytes expressing untagged ATP1A3-containing Na^+/K^+-ATPases are shown. The blue line represents the monoexponential decay function obtained by fitting the off-transient current starting 4 ms after the end of the voltage pulse. (B) Charge-voltage plots of off-transient currents. Transient currents induced by the return from each voltage pulse to the holding potential of 0 mV were fit to monoexponential decay curves and integrated to yield the charge moved Q shown on the Y-axis. Owing to the small magnitude of p.V130del transient currents, the same curve is shown at larger scale at the bottom.

Figure 4 p.V130del ATP1A3 Is Expressed and Reaches the Cell Surface

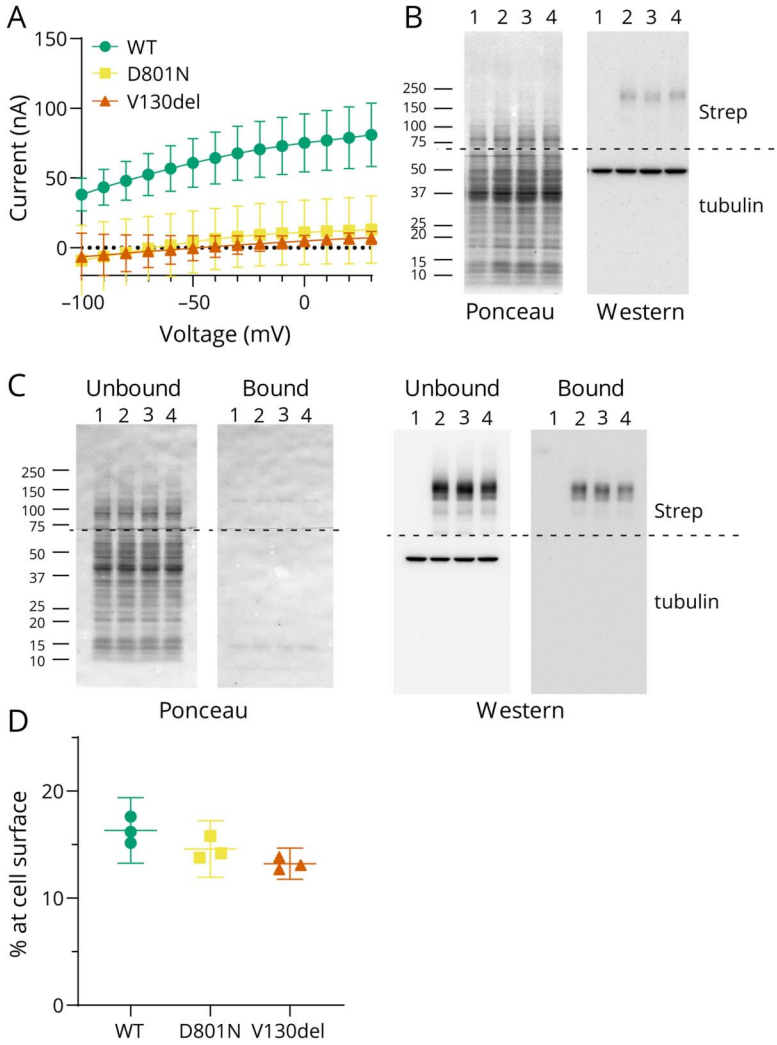

(A) An N-terminal tag does not disrupt ATP1A3 function. N-FLAG-Strep-mCherry-tagged ATP1A3 constructs were expressed in *Xenopus* oocytes. Na^+/K^+-ATPase-specific electrogenic ion transport currents in the presence of 5 mM extracellular K^+, measured as in Figure 2C, are shown. (B) Representative Western blot of oocytes expressing N-tagged ATP1A3 shows that p.V130del proteins are expressed. A constant amount of total protein was loaded in each lane and visualized by Ponceau stain before blocking (left). The blots were then cut in half (dotted line). The top half was probed using anti-Strep tag primary antibody to detect tagged ATP1A3 (expected size ~146 kDa including 34 kDa tag), and the bottom half was probed using anti-α-tubulin primary antibody as an additional loading control; the 2 halves are shown together. Lane 1: uninjected negative control; 2: wildtype, 3: p.D801N, 4: p.V130del. (C) Cell surface biotinylation followed by avidin pulldown demonstrates N-tagged p.V130del ATP1A3 at the cell surface. Oocytes expressing the indicated N-tagged construct were treated with a cell surface biotinylation reagent. Avidin chromatography was performed to separate cell surface (bound) and intracellular (unbound) protein fractions for Western blot. More total protein was present in the unbound than the bound fraction, as shown by the Ponceau stain of the blots before blocking at left. The blots were then cut in half and probed against anti-Strep/anti-tubulin; lanes are numbered as in (B). (D) Semiquantitative determination of band intensity from cell surface biotinylation assays, normalized to the total amount of detected ATP1A3 as detailed in the Methods. All 3 ATP1A3 proteins were present at the cell surface.

detectable in only the unbound and not the avidin-bound fraction (Figure 4C, bottom right). Semiquantitative determination of band intensity suggested a mild decrease in the proportion of p.V130del reaching the cell surface (Figure 4D). Potential sources of error that prevented precise quantitation included variability in expression between oocytes and the possibility that avidin pull-down of ATP1A3 occurred through its interaction with the β subunit, which has far more extracellular lysines available for labeling. However, the presence of p.V130del ATP1A3 at the cell surface was clearly out of proportion to the complete loss of ion transport activity seen in the two-electrode voltage clamp, indicating that p.V130del eliminates enzyme function independently of any additional effects on protein folding or trafficking.

Discussion

Recurrent encephalopathy as the presenting feature of *ATP1A3*-related disease has primarily been described in the form of fever-triggered episodes with ataxia and/or generalized weakness (RECA, FIPWE), linked to variants at p.R756. We expand the spectrum of *ATP1A3*-related recurrent encephalopathy to include episodes not triggered by fever in a patient with a different variant, p.V130del. Multiple lines of evidence including clinical information, cell survival assay, and electrophysiology indicate that p.V130del is pathogenic with a loss-of-function effect that eliminates enzyme function but not protein expression.

Our experimental observation is that loss of Val130 disrupts ion transport and Na^+ binding is consistent with its location in the protein structure. p.V130del represents in-frame loss of either of 2 consecutive valine residues that share the same codon, Val129-Val130; the deletion was assigned to position 130 following the 3′ rule.[32] Of interest, a pathogenic missense variant affecting the same position, NM_152296.4: c.385G>A; p.(V129M), has previously been reported in an individual with *ATP1A3*-related childhood-onset schizophrenia.[33] Val129-Val130 lie within the transmembrane ion-binding domain in transmembrane helix M2, which interacts

with helix M1, runs alongside 2 helices (M4 and M6) that form the ion-binding sites (Figure 1), and rotates relative to the latter during each catalytic cycle.[24,34] Deletion of one valine might displace the rest of the M2 side chains by 100°, disrupting these interactions, or distorting the local protein structure including the M4 and M6 surfaces that interact with bound ions. Such an effect on ion binding would be consistent with the small, abnormal Na^+ transient currents seen with p.V130del. However, a limitation of the two-electrode voltage clamp system is that we could not determine how many Na^+ the enzyme bound, leaving 2 possible scenarios. p.V130del might alter the apparent affinity for extracellular Na^+ and slow the Na^+ binding/unbinding steps of the reaction cycle; alternatively, p.V130del might eliminate one Na^+ binding site so that ion transport becomes electroneutral (2 Na^+:2 K^+) and undetectable by electrophysiologic methods. Even if electroneutral exchange is occurring, however, cell death in the ouabain survival assay shows that it cannot replace normal enzyme activity.

The lack of a fever trigger in our patient expands the phenotype of *ATP1A3*-related recurrent encephalopathy. Most patients with encephalopathic episodes as the predominant feature of *ATP1A3* disease have a recognizable syndrome in which infrequent, slowly recovering episodes of acute encephalopathy are triggered by fever and may be accompanied by ataxia and/or generalized weakness (RECA/FIPWE). Many of these individuals also develop nonparoxysmal symptoms such as hyperkinetic movement disorders, as typical in *ATP1A3*-related disease, but the encephalopathic episodes and accompanying motor deficits are the key features. This syndrome has displayed a strong genotype-phenotype correlation with p.R756H, p.R756C, or p.R756L variants in more than 10 independent reports to date from our group and others.[14,35–51] Remarkably, fever consistently precedes encephalopathic episodes among all these patients, suggesting that hyperthermia or infection/inflammation could be specific triggers. p.R756H was recently discovered to induce misfolding of ATP1A3 at elevated temperatures, providing a biochemical explanation for intermittent hyperthermia-triggered symptoms in these patients. The p.R756H variant enzyme functions at about half the wildtype enzymatic turnover rate at 37°C, but disappears from the cell surface and loses enzymatic activity at 39°C.[13]

In comparison with the p.R756 phenotype, our patient has the same core features—infrequent, slowly recovering episodes of encephalopathy with weakness—but with 2 episodes not triggered by fever. This finding provides additional, indirect support for the pathologic relevance of p.R756H temperature sensitivity: Unlike p.R756H, p.V130del enzymes are completely nonfunctional even at low temperatures in vitro, and their resulting phenotype is not temperature-dependent. One limitation of our study is that because oocytes are unstable at higher temperatures, we could not determine whether p.V130del enzymes are also sensitive to hyperthermia in this model system. However, p.V130del enzymes already have zero activity even when they reach the cell surface, so any such intermittent pathogenic effect would need to induce toxic gain-of-function or dominant negativity. Another possibility is that reduction of total Na^+/K^+-ATPase activity in neurons heterozygous for p.V130del lowers their threshold for slowly recovering or self-propagating pathologies such as excitotoxicity or spreading depression.

The relatively mild phenotype of p.V130del provides further support for the hypothesis that haploinsufficiency alone causes mild phenotypes in Na^+/K^+-ATPase disorders, whereas more severe phenotypes involve additional mechanisms such as protein toxicity. In our patient, haploinsufficiency with heterozygosity for an allele exhibiting total loss-of-function in vitro resulted in occasional episodes of neurologic dysfunction with mild nonparoxysmal features and otherwise typical development. By contrast, some missense variants found to induce toxic endoplasmic reticulum stress or dominant-negative interference with wildtype Na^+/K^+-ATPase activity cause more severe AHC phenotypes with frequent episodes, severe nonparoxysmal features, and intellectual disability.[31,52,53] Similarly, we have observed that heterozygous null variants in the paralogous *ATP1A1* gene, which encodes the ubiquitously expressed isoform of the Na^+/K^+-ATPase α subunit, can be nonpenetrant in humans and mice (manuscript under review). We conclude that the *ATP1A3* phenotypic spectrum includes individuals who are mildly affected in comparison with AHC and have few nonparoxysmal features. *ATP1A3*-related disease should be considered in the differential diagnosis of patients with recurrent episodes of encephalopathy and weakness, regardless of whether the episodes are triggered by fever.

Acknowledgment

The authors thank the family for their participation in this study. Molecular graphics and analyses were performed with UCSF ChimeraX, developed by the Resource for Biocomputing, Visualization, and Informatics at the University of California, San Francisco, with support from National Institutes of Health R01-GM129325 and the Office of Cyber Infrastructure and Computational Biology, National Institute of Allergy and Infectious Diseases.

Study Funding

The authors report no targeted funding.

Disclosure

C. Immanneni was supported by the NIH Intramural Research Program. D. Calame was supported by NIH Brain Disorders and Development Training Grant (T32 NS043124-19) and Muscular Dystrophy Association (MDA) Grant 873841. S. Jiao is supported by the NIH Intramural Research Program. M. Holmgren is supported by the NIH Intramural Research Program. S. Yano serves as an associate editor for the journal Molecular Genetics & Genomic Medicine and was supported by the NIH Intramural Research Program. Go to Neurology.org/NG for full disclosures.

Publication History

Received by *Neurology: Genetics* October 20, 2023. Accepted in final form February 23, 2024. Submitted and externally peer reviewed. The handling editor was Associate Editor Alexandra Durr, MD, PhD.

Appendix Authors

Name	Location	Contribution
Chetan Immanneni, BA	Sam Houston State University College of Osteopathic Medicine, Conroe, TX; Molecular Neurophysiology Unit, National Institute of Neurological Diseases and Stroke, National Institutes of Health, Bethesda, MD	Drafting/revision of the manuscript for content, including medical writing for content; major role in the acquisition of data; analysis or interpretation of data
Daniel Calame, MD, PhD	Section of Pediatric Neurology and Developmental Neuroscience, Department of Pediatrics; Department of Molecular and Human Genetics, Baylor College of Medicine; Texas Children's Hospital, Houston, TX	Drafting/revision of the manuscript for content, including medical writing for content; major role in the acquisition of data; study concept or design; analysis or interpretation of data
Song Jiao, PhD	Molecular Neurophysiology Unit, National Institute of Neurological Diseases and Stroke, National Institutes of Health, Bethesda, MD	Drafting/revision of the manuscript for content, including medical writing for content; major role in the acquisition of data; study concept or design; analysis or interpretation of data
Lisa T. Emrick, MD	Department of Molecular and Human Genetics, Baylor College of Medicine, Houston, TX	Drafting/revision of the manuscript for content, including medical writing for content; study concept or design; analysis or interpretation of data
Miguel Holmgren, PhD	Molecular Neurophysiology Unit, National Institute of Neurological Diseases and Stroke, National Institutes of Health, Bethesda, MD	Drafting/revision of the manuscript for content, including medical writing for content; study concept or design; analysis or interpretation of data
Sho T. Yano, MD, PhD	National Human Genome Research Institute, National Institutes of Health, Bethesda, MD; Section of Pediatric Neurology, Department of Pediatrics, University of Chicago, IL	Drafting/revision of the manuscript for content, including medical writing for content; major role in the acquisition of data; study concept or design; analysis or interpretation of data

References

1. Clausen MV, Hilbers F, Poulsen H. The structure and function of the Na,K-ATPase isoforms in health and disease. *Front Physiol.* 2017;8:371. doi:10.3389/fphys.2017.00371
2. Jiao S, Johnson K, Moreno C, Yano S, Holmgren M. Comparative description of the mRNA expression profile of Na(+)/K(+) -ATPase isoforms in adult mouse nervous system. *J Comp Neurol.* 2022;530(3):627-647. doi:10.1002/cne.25234
3. Heinzen EL, Swoboda KJ, Hitomi Y, et al. De novo mutations in ATP1A3 cause alternating hemiplegia of childhood. *Nat Genet.* 2012;44(9):1030-1034. doi:10.1038/ng.2358
4. Rosewich H, Thiele H, Ohlenbusch A, et al. Heterozygous de-novo mutations in ATP1A3 in patients with alternating hemiplegia of childhood: a whole-exome sequencing gene-identification study. *Lancet Neurol.* 2012;11(9):764-773. doi:10.1016/S1474-4422(12)70182-5
5. de Carvalho Aguiar P, Sweadner KJ, Penniston JT, et al. Mutations in the Na+/K+ -ATPase alpha3 gene ATP1A3 are associated with rapid-onset dystonia parkinsonism. *Neuron.* 2004;43(2):169-175. doi:10.1016/j.neuron.2004.06.028
6. Demos MK, van Karnebeek CD, Ross CJ, et al. A novel recurrent mutation in ATP1A3 causes CAPOS syndrome. *Orphanet J Rare Dis.* 2014;9:15. doi:10.1186/1750-1172-9-15
7. Miyatake S, Kato M, Kumamoto T, et al. De novo ATP1A3 variants cause polymicrogyria. *Sci Adv.* 2021;7(13):eabd2368. doi:10.1126/sciadv.abd2368
8. Vetro A, Nielsen HN, Holm R, et al. ATP1A2- and ATP1A3-associated early profound epileptic encephalopathy and polymicrogyria. *Brain.* 2021;144(5):1435-1450. doi:10.1093/brain/awab052
9. Prange L, Pratt M, Herman K, et al. D-DEMØ, a distinct phenotype caused by ATP1A3 mutations. *Neurol Genet.* 2020;6(5):e466. doi:10.1212/NXG.0000000000000466
10. Han KH, Oh DY, Lee S, et al. ATP1A3 mutations can cause progressive auditory neuropathy: a new gene of auditory synaptopathy. *Sci Rep.* 2017;7(1):16504. doi:10.1038/s41598-017-16676-9
11. Roenn CP, Li M, Schack VR, et al. Functional consequences of the CAPOS mutation E818K of Na(+),K(+)-ATPase. *J Biol Chem.* 2019;294(1):269-280. doi:10.1074/jbc.RA118.004591
12. Lazarov E, Hillebrand M, Schroder S, et al. Comparative analysis of alternating hemiplegia of childhood and rapid-onset dystonia-parkinsonism ATP1A3 mutations reveals functional deficits, which do not correlate with disease severity. *Neurobiol Dis.* 2020;143:105012. doi:10.1016/j.nbd.2020.105012
13. Arystarkhova E, Toustrup-Jensen MS, Holm R, et al. Temperature instability of a mutation at a multidomain junction in Na,K-ATPase isoform ATP1A3 (p.Arg756His) produces a fever-induced neurological syndrome. *J Biol Chem.* 2023;299(1):102758. doi:10.1016/j.jbc.2022.102758
14. Dard R, Mignot C, Durr A, et al. Relapsing encephalopathy with cerebellar ataxia related to an ATP1A3 mutation. *Dev Med Child Neurol.* 2015;57(12):1183-1186. doi:10.1111/dmcn.12927
15. Moreno C, Jiao S, Yano S, Holmgren M. Disease mutations of human α3 Na^+/K^+-ATPase define extracellular Na^+ binding/occlusion kinetics at ion binding site III. *PNAS Nexus.* 2022;1(4):pgac205. doi:10.1093/pnasnexus/pgac205
16. Liman ER, Tytgat J, Hess P. Subunit stoichiometry of a mammalian K+ channel determined by construction of multimeric cDNAs. *Neuron.* 1992;9(5):861-871. doi:10.1016/0896-6273(92)90239-a
17. Addgene. Accessed April 13, 2024. n2t.net/addgene:68375
18. Dalvai M, Loehr J, Jacquet K, et al. A scalable genome-Editing-based approach for mapping multiprotein complexes in human cells. *Cell Rep.* 2015;13(3):621-633. doi:10.1016/j.celrep.2015.09.009
19. Addgene. Accessed April 13, 2024. n2t.net/addgene:41583
20. Gurtan AM, Lu V, Bhutkar A, Sharp PA. In vivo structure-function analysis of human Dicer reveals directional processing of precursor miRNAs. *RNA.* 2012;18(6):1116-1122. doi:10.1261/rna.032680.112
21. Lopez-Rodriguez A, Holmgren M. Restoration of proper trafficking to the cell surface for membrane proteins harboring cysteine mutations. *PLoS One.* 2012;7(10):e47693. doi:10.1371/journal.pone.0047693
22. Harris M, Garcia-Caballero A, Stutts MJ, Firsov D, Rossier BC. Preferential assembly of epithelial sodium channel (ENaC) subunits in Xenopus oocytes: role of furin-mediated endogenous proteolysis. *J Biol Chem.* 2008;283(12):7455-7463. doi:10.1074/jbc.M707399200
23. Meyer DJ, Gatto C, Artigas P. On the effect of hyperaldosteronism-inducing mutations in Na/K pumps. *J Gen Physiol.* 2017;149(11):1009-1028. doi:10.1085/jgp.201711827
24. Kanai R, Ogawa H, Vilsen B, Cornelius F, Toyoshima C. Crystal structure of a Na+-bound Na+,K+-ATPase preceding the E1P state. *Nature.* 2013;502(7470):201-206. doi:10.1038/nature12578
25. Pettersen EF, Goddard TD, Huang CC, et al. UCSF ChimeraX: structure visualization for researchers, educators, and developers. *Protein Sci.* 2021;30(1):70-82. doi:10.1002/pro.3943
26. Berman HM, Westbrook J, Feng Z, et al. The protein data bank. *Nucleic Acids Res.* 2000;28(1):235-242. doi:10.1093/nar/28.1.235
27. Blanchette M, Kent WJ, Riemer C, et al. Aligning multiple genomic sequences with the threaded blockset aligner. *Genome Res.* 2004;14(4):708-715. doi:10.1101/gr.1933104
28. Kent WJ, Sugnet CW, Furey TS, et al. The human genome browser at UCSC. *Genome Res.* 2002;12(6):996-1006. doi:10.1101/gr.229102
29. Richards S, Aziz N, Bale S, et al. Standards and guidelines for the interpretation of sequence variants: a joint consensus recommendation of the American College of Medical Genetics and Genomics and the Association for Molecular Pathology. *Genet Med.* 2015;17(5):405-424. doi:10.1038/gim.2015.30
30. Brnich SE, Abou Tayoun AN, Couch FJ, et al. Recommendations for application of the functional evidence PS3/BS3 criterion using the ACMG/AMP sequence variant interpretation framework. *Genome Med.* 2019;12(1):3. doi:10.1186/s13073-019-0690-2
31. Li M, Jazayeri D, Corry B, et al. A functional correlate of severity in alternating hemiplegia of childhood. *Neurobiol Dis.* 2015;77:88-93. doi:10.1016/j.nbd.2015.02.002
32. den Dunnen JT, Dalgleish R, Maglott DR, et al. HGVS recommendations for the description of sequence variants: 2016 update. *Hum Mutat.* 2016;37(6):564-569. doi:10.1002/humu.22981
33. Smedemark-Margulies N, Brownstein CA, Vargas S, et al. A novel de novo mutation in ATP1A3 and childhood-onset schizophrenia. *Cold Spring Harb Mol Case Stud.* 2016;2(5):a001008. doi:10.1101/mcs.a001008
34. Nguyen PT, Deisl C, Fine M, et al. Structural basis for gating mechanism of the human sodium-potassium pump. *Nat Commun.* 2022;13(1):5293. doi:10.1038/s41467-022-32990-x

35. Brashear A, Mink JW, Hill DF, et al. ATP1A3 mutations in infants: a new rapid-onset dystonia-Parkinsonism phenotype characterized by motor delay and ataxia. *Dev Med Child Neurol.* 2012;54(11):1065-1067. doi:10.1111/j.1469-8749.2012.04421.x
36. Fornarino S, Stagnaro M, Rinelli M, et al. Paroxysmal features responding to flunarizine in a child with rapid-onset dystonia-parkinsonism. *Neurology*. 2014;82(22):2037-2038. doi:10.1212/WNL.0000000000000473
37. Tan AH, Ozelius LJ, Brashear A, et al. Rapid-onset dystonia-parkinsonism in a Chinese girl with a de novo ATP1A3 c.2267G>A (p.R756H) genetic mutation. *Mov Disord Clin Pract.* 2015;2(1):74-75. doi:10.1002/mdc3.12122
38. de Gusmao CM, Dy M, Sharma N. Beyond dystonia-parkinsonism: chorea and ataxia with ATP1A3 mutations. *Mov Disord Clin Pract.* 2016;3(4):402-404. doi:10.1002/mdc3.12317
39. Kanemasa H, Fukai R, Sakai Y, et al. De novo p.Arg756Cys mutation of ATP1A3 causes an atypical form of alternating hemiplegia of childhood with prolonged paralysis and choreoathetosis. *BMC Neurol.* 2016;16:174. doi:10.1186/s12883-016-0680-6
40. Nicita F, Travaglini L, Sabatini S, et al. Childhood-onset ATP1A3-related conditions: report of two new cases of phenotypic spectrum. *Parkinsonism Relat Disord.* 2016;30:81-82. doi:10.1016/j.parkreldis.2016.05.029
41. Hully M, Ropars J, Hubert L, et al. Mosaicism in ATP1A3-related disorders: not just a theoretical risk. *Neurogenetics*. 2017;18(1):23-28. doi:10.1007/s10048-016-0498-9
42. Jaffer F, Fawcett K, Sims D, et al. Familial childhood-onset progressive cerebellar syndrome associated with the ATP1A3 mutation. *Neurol Genet.* 2017;3(2):e145. doi:10.1212/NXG.0000000000000145
43. Sousa AL, Alonso I, Magalhaes M. A Portuguese rapid-onset dystonia-Parkinsonism case with atypical features. *Neurol Sci.* 2017;38(9):1713-1714. doi:10.1007/s10072-017-2996-4
44. Yano ST, Silver K, Young R, et al. Fever-induced paroxysmal weakness and encephalopathy, a new phenotype of ATP1A3 mutation. *Pediatr Neurol.* 2017;73:101-105. doi:10.1016/j.pediatrneurol.2017.04.022
45. Nakamura Y, Hattori A, Nakashima M, et al. A de novo p.Arg756Cys mutation in ATP1A3 causes a distinct phenotype with prolonged weakness and encephalopathy triggered by fever. *Brain Dev.* 2018;40(3):222-225. doi:10.1016/j.braindev.2017.09.010
46. Schirinzi T, Graziola F, Nicita F, et al. Childhood rapid-onset ataxia: expanding the phenotypic spectrum of ATP1A3 mutations. *Cerebellum*. 2018;17(4):489-493. doi:10.1007/s12311-018-0920-y
47. Sival DA, Vansenne F, Van der Hout AH, Tijssen MAJ, de Koning TJ. Fever-induced paroxysmal weakness and encephalopathy (FIPWE)-Part of a phenotypic continuum in patients with ATP1A3 mutations? *Pediatr Neurol.* 2018;81:57-58. doi:10.1016/j.pediatrneurol.2017.12.009
48. Sabouraud P, Riquet A, Spitz MA, et al. Relapsing encephalopathy with cerebellar ataxia are caused by variants involving p.Arg756 in ATP1A3. *Eur J Paediatr Neurol.* 2019;23(3):448-455. doi:10.1016/j.ejpn.2019.02.004
49. Biela M, Rydzanicz M, Szymanska K, et al. Variants of ATP1A3 in residue 756 cause a separate phenotype of relapsing encephalopathy with cerebellar ataxia (RECA)-Report of two cases and literature review. *Mol Genet Genomic Med.* 2021;9(9):e1772. doi:10.1002/mgg3.1772
50. De Vrieze J, van de Laar I, de Rijk-van Andel JF, Kamsteeg EJ, Kotsopoulos IAW, de Man SA. Expanding phenotype of *ATP1A3* - related disorders: a case series. *Child Neurol Open.* 2021;8:2329048X211048068. doi:10.1177/2329048X211048068
51. Zhang W, Li J, Zhuo X, et al. Chinese patients with p.Arg756 mutations of ATP1A3: clinical manifestations, treatment, and follow-up. *Pediatr Investig.* 2022;6(1):5-10. doi:10.1002/ped4.12310
52. Arystarkhova E, Haq IU, Luebbert T, et al. Factors in the disease severity of ATP1A3 mutations: impairment, misfolding, and allele competition. *Neurobiol Dis.* 2019;132:104577. doi:10.1016/j.nbd.2019.104577
53. Arystarkhova E, Ozelius LJ, Brashear A, Sweadner KJ. Misfolding, altered membrane distributions, and the unfolded protein response contribute to pathogenicity differences in Na,K-ATPase ATP1A3 mutations. *J Biol Chem.* 2021;296:100019. doi:10.1074/jbc.RA120.015271